

Generation of coherent terahertz pulses in ruby at room temperature

Elena Kuznetsova,¹ Yuri Rostovtsev,¹ Nikolai G. Kalugin,¹ Roman Kolesov,¹ Olga Kocharovskaya,¹ and Marlan O. Scully^{1,2}

¹*Institute for Quantum Studies and Department of Physics, Texas A&M University, College Station, Texas 77843, USA*

²*Princeton Institute for Material Science and Department of Mechanical and Aerospace Engineering,*

Princeton University, New Jersey 08544, USA

(Received 8 May 2006; published 29 August 2006)

We have shown that a coherently driven solid state medium can potentially produce strong controllable short pulses of THz radiation. The high efficiency of the technique is based on excitation of maximal THz coherence by applying resonant optical pulses to the medium. The excited coherence in the medium is connected to macroscopic polarization coupled to THz radiation. We have performed detailed simulations by solving the coupled density matrix and Maxwell equations. By using a simple V-type energy scheme for ruby, we have demonstrated that the energy of generated THz pulses ranges from hundreds of pico-Joules to nano-Joules at room temperature and micro-Joules at liquid helium temperature, with pulse durations from picoseconds to tens of nanoseconds. We have also suggested a coherent ruby source that lases on two optical wavelengths and simultaneously generates THz radiation. We discussed also possibilities of extension of the technique to different solid-state materials.

DOI: 10.1103/PhysRevA.74.023819

PACS number(s): 42.50.Gy, 42.65.Ky

I. INTRODUCTION

The search for efficient, high-power, inexpensive, compact, and room-temperature methods of generation of coherent terahertz (THz) radiation is one of the main topics in modern optoelectronics and photonics [1]. Its importance is based on the fact that THz radiation has unique potential for a wide range of applications from diagnostics of different materials (including semiconductors, chemical compounds, biomolecules, and biotissues), imaging (for medical and security purposes), to remote atmospheric sensing and monitoring, astronomy, etc. [2,3].

In previous works we have focussed on a new approach to the problem of generation of short coherent THz pulsed radiation by taking advantage of dramatic enhancement of the nonlinear response of a medium via maximal quantum coherence [4–6], created in atomic and molecular gases with different level configurations (double- Λ , V- Λ , double-V schemes) by coherent laser radiation.

As is well known, quantum coherence can dramatically change the optical properties of media. For example, lasing without population inversion (LWI) [7] and electromagnetically induced transparency (EIT) [8] have been demonstrated [9,10] in coherently driven media. These unusual properties are employed for generation of electromagnetic radiation of different frequencies ranging from IR [11,12] to UV [13], and γ rays [14]. Enhancement of coherent Raman scattering via maximal coherence has been demonstrated experimentally [15], and it has applications to enhanced real time spectroscopy (FAST CARS) [16]. Previously, the double Λ scheme with near-maximal Raman coherence was used for highly efficient conversion of blue to ultraviolet light in Pb vapor [13]. A new type of gas-phase optical parametric oscillator [11] was suggested for frequency down conversion to generate 1.88 μm radiation in Pb vapor, and efficient infrared upconversion [12] was suggested to convert infrared light with a 100 μm wavelength to the visible. The first experimental demonstration supporting these ideas was per-

formed in Ref. [4], where 5 μm IR radiation was generated in Rb atomic vapor.

Many results in this area have been obtained in gases, but, recently, EIT has been generalized and extended to solids with a long-lived spin coherence [17], a class of solid materials, namely, rare-earth, and transition metal ion doped dielectrics have been suggested as very attractive from the point of view of realization and applications of EIT. Several applications of EIT to improve performance of solid state lasers have been already proposed [18,19]. LWI, first realized in a gas medium [9], recently has been demonstrated in solids as well [20].

In this paper we extend the approach of generation of THz radiation via resonantly induced coherence to solid state media. The coherence at the corresponding transition can be induced by coherent optical fields as shown in Fig. 1. Electronic levels of the THz transition are coupled by a pair of optical fields with Rabi frequencies Ω_1 and Ω_2 to a common ground state forming a V system of energy levels. Coherence ρ_{cb} induced by the optical fields at the THz transition gives rise to polarization provided that the corresponding dipole moment is not zero, which will radiate out a THz pulse with

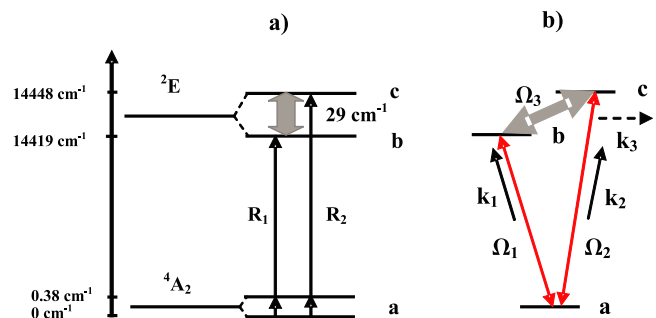


FIG. 1. (Color online) (a) Three-level V energy system in ruby proposed for generation of 29 cm^{-1} THz pulses, (b) Model V system of energy levels with two copropagating fields 1 and 2 inducing coherence between levels b and c .

Rabi frequency Ω_3 . This method differs from the one proposed in Refs. [5,6] for gaseous media where the optically prepared THz coherence produces no macroscopic polarization of gaseous media at a THz transition (this is the manifestation of symmetry with respect to inversion), the reason is that an electrically allowed dipole moment at the two-photon transition is zero since it is typically forbidden (although, it is important to note here that the magnetic dipole moment can be nonzero even in gases, we discuss this opportunity later). For doped solids having sites with no inversion symmetry is common, such as the one occupied by Cr^{3+} [simplified energy level structure is shown in Fig. 1(a)] in ruby, the corresponding two-photon transition dipole moment is not zero, resulting in all three transitions in the V scheme being allowed. It is worth mentioning that using nonlinear optical mixing in a semiconductor heterostructure for generation of few-cycle THz pulses was proposed in Ref. [21].

In ruby closely spaced R_1 and R_2 lines arise from transitions between the ground state of the Cr^{3+} ion (4A_2) and its first excited state (2E). Each of these cubic-field states is split by the trigonal crystal field and spin-orbit coupling into a pair of Kramers doublets, 0.38 cm^{-1} apart in the ground state and 29.14 cm^{-1} apart in the 2E state. The width of the R lines is about 11 cm^{-1} at room temperature and 0.15 cm^{-1} at the temperature of liquid nitrogen. The transitions from the 4A_2 ground state to levels 2E are spin-forbidden, and have oscillator strength $\sim 7.5 \times 10^{-7}$ [R_1, R_2 line peak cross section is $\sim (1.2-1.4) \times 10^{-18} \text{ cm}^2$ at the temperature of liquid nitrogen and $\sim 4 \times 10^{-20} \text{ cm}^2$ at room temperature]. They are predominantly electric-dipole in nature, since the inversion symmetry of a cubic crystal field is broken by crystal field trigonal distortions and odd-parity lattice vibrations. Namely, the odd-parity component of the crystal field at the Cr^{3+} ion mixes odd-parity states of high energy into the even parity d states between which R transitions are observed and makes them weakly allowed. The magnetic-dipole contribution to the R lines is estimated to be $\sim 1/30$ of the strength of the electric-dipole transitions [22].

The 29 cm^{-1} transition in ruby has history which is as rich as the ruby laser itself. It was considered promising for realization of a quantum counter for far-infrared radiation (FIR) [23] on one hand, and as a system very convenient to study interaction processes of nonequilibrium phonons with two-level electronic systems (so-called phonon spectrometer), on the other [24]. There was also a proposal to make a far-infrared laser at this transition pumping via the R_2 line, but due to the unfavorable ratio of relaxation rates (fast relaxation at the FIR and slow at the optical R_1 transition), the laser could operate only at liquid helium temperature and the estimated gain did not exceed losses [25].

It is interesting that 29 cm^{-1} FIR was produced by nonlinear mixing of two ruby laser beams, one emitting at R_1 and another at R_2 , in LiNbO_3 [26] and in ZnTe crystals [27], with the efficiency $\eta \sim 10^{-9}$. The method proposed in the present work would allow pulsed THz radiation to be easily produced from a dual-color ruby laser itself, operating at both R_1 and R_2 lines, thus significantly miniaturizing the system.

The outline of the paper is the following. In the next section we describe a theoretical model used to calculate

parameters of generated THz pulses. In Sec. III we consider possibilities of phase matching for fields in different regimes (CW and short pulses). In Sec. IV we make estimates showing the perspective of the suggested scheme as well as discuss a proposed experiment with a standard laser setup. Next we show that the system we have considered is not limited, i.e., there are many systems to which our theory can be applied. Finally we compare the efficiency of our scheme with the methods of generation of THz radiation used nowadays and possible applications that are opened due to the high efficiency of the proposed technique.

II. THEORETICAL MODEL

A. Real system

The ruby system shown in Fig. 1(a) includes eight states, four in the ground 4A_2 and four in the excited 2E one. In our theoretical analysis we describe it using only three levels as in Fig. 1(b), since this simple model takes into account all essential physics and allows us to make estimates of expected THz radiation characteristics and required optical field parameters.

For the proposed technique to work we need to make sure that an efficient V scheme can be realized. In the case of a single fs pulse, driving both optical transitions simultaneously, we will have only one polarization, for example, linear. For two pulses we can choose each pulse polarization separately. Selection rules for the right circular and left circular polarizations are shown in Fig. 2(a) [28]. As one can see, neither for the right, nor for the left circular polarization a V scheme involving R_1 and R_2 transitions can be organized. For a linear polarization perpendicular to the optic axis, which is an equal sum or difference of the right and left ones, there are four V schemes possible, shown in Fig. 2(b).

Taking into account the relation between the coefficients C^+ and C^- : $C^+C^{-*} = -C^-C^{+*}$, one can see that the schemes A and C cancel each other, since the products of the matrix elements are opposite ($\pm 4C^+C^{-*}/9$ for A and C, respectively). On the other hand, for schemes B and D the products are the same ($-2\sqrt{2}C^+C^{-*}/9$). These two V schemes will interfere constructively and induce the THz coherence.

B. Simplified model

The interaction Hamiltonian for the system shown in Fig. 1(b) is given by

$$V_I = -\hbar[\Omega_1 e^{-i\omega_{ba}t}|b\rangle\langle a| + \Omega_2 e^{-i\omega_{ca}t}|c\rangle\langle a| + \text{H.c.}] \\ -\hbar[\Omega_3 e^{-i\omega_{cb}t}|c\rangle\langle b| + \text{H.c.}], \quad (1)$$

where $\Omega_i = p_{\mu\nu} \mathcal{E}_i / \hbar$ is the Rabi frequency of the respective field, $\mu\nu = ba, ca, cb$ and $i = 1, 2, 3$; p_{ba} and p_{ca} are the electric dipole matrix elements of the optical transitions $b \leftrightarrow a$ and $c \leftrightarrow a$, and p_{cb} of the THz transition $c \leftrightarrow b$, respectively; ω_{ba} , ω_{ca} , and ω_{cb} are the frequencies of the electronic and THz transitions; \mathcal{E}_i is the amplitude of the respective electromagnetic field.

The time-dependent density matrix equations are

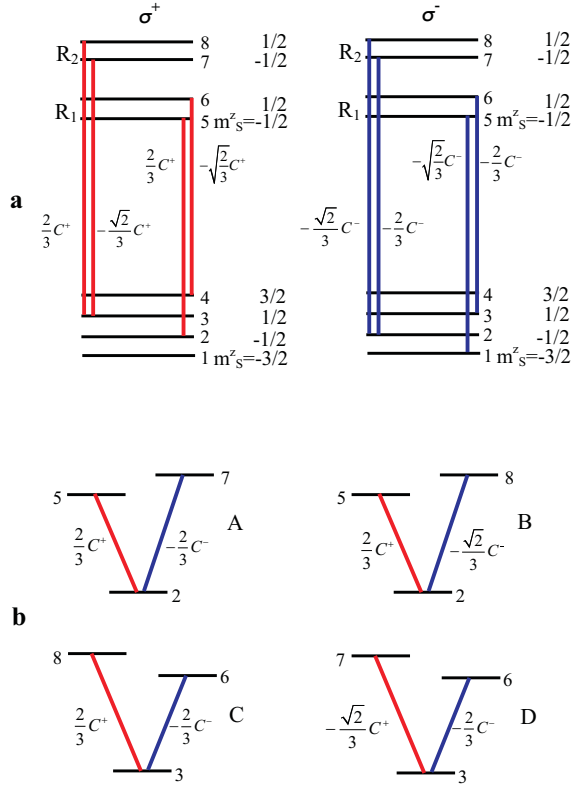


FIG. 2. (Color online) (a) Selection rules and transition matrix elements for R_1 and R_2 optical transitions in ruby for right and left circular polarizations, (b) Four V schemes possible for linearly polarized fields.

$$\frac{\partial \rho}{\partial t} = -\frac{i}{\hbar}[H, \rho] - \frac{1}{2}(\Gamma \rho + \rho \Gamma), \quad (2)$$

where Γ is the relaxation matrix and H is the total Hamiltonian. To estimate the efficiency of THz radiation generation and required laser field intensities we first consider the system (2) in the limit of ultrashort pulses, which are short compared to relaxation times of the system, and neglect propagation effects for the optical fields. In this simplified picture we assume that the system is driven by two resonant fields with equal time-dependent Rabi frequencies $\Omega_1 = \Omega_2 = \Omega(t)$ (assumed real). In the case of a V scheme considered in this work the STIRAP technique, proposed in Refs. [5,6] for maximal molecular coherence excitation in a Λ energy system, is not applicable. In the case of the V scheme maximal coherence is excited by two fields of equal Rabi frequency and duration, acting simultaneously. The system is then described by the following set of equations:

$$\frac{d\sigma_{ca}}{dt} = i\Omega(\rho_a - \rho_c) - i\Omega\sigma_{cb}, \quad (3)$$

$$\frac{d\sigma_{ba}}{dt} = i\Omega(\rho_a - \rho_b) - i\Omega\sigma_{cb}^*, \quad (4)$$

$$\frac{d\sigma_{cb}}{dt} = i\Omega(\sigma_{ba}^* - \sigma_{ca}), \quad (5)$$

$$\frac{d\rho_a}{dt} = i\Omega(\sigma_{ba} + \sigma_{ca}) - i\Omega(\sigma_{ba}^* + \sigma_{ca}^*), \quad (6)$$

$$\frac{d\rho_b}{dt} = i\Omega(\sigma_{ba}^* - \sigma_{ba}), \quad (7)$$

$$\rho_c = 1 - \rho_a - \rho_b. \quad (8)$$

Due to the symmetry of the model system $\rho_b = \rho_c$, $\sigma_{ba} = \sigma_{ca}$, and σ_{cb} is real. Let us introduce new variables

$$\alpha = (\sigma_{ba} + \sigma_{ca})/2 = \sigma_{ba}, \quad (9)$$

$$\beta = (\sigma_{cb} + \sigma_{cb}^*)/2 = \text{Re}(\sigma_{cb}) = \sigma_{cb}, \quad (10)$$

for which, taking into account Eqs. (5) and (6), the following relation can be obtained:

$$\frac{d}{dt}(\rho_a + 2\beta) = 0, \quad (11)$$

giving $\rho_a + 2\beta = 1$. For the new variables we arrive at the following system of equations

$$\frac{d\alpha}{dt} = i\Omega - 4i\Omega\beta, \quad (12)$$

$$\frac{d\beta}{dt} = 2i\Omega(\alpha^* - \alpha), \quad (13)$$

which can be further simplified if we substitute $\xi = \alpha - \alpha^*$

$$\frac{d\xi}{dt} = 2i\Omega - 8i\Omega\beta, \quad (14)$$

$$\frac{d\beta}{dt} = -2i\Omega\xi. \quad (15)$$

The solution of this system is

$$\xi = \frac{\sqrt{2}i}{2} \sin\left(2\sqrt{2} \int_{-\infty}^t \Omega(t') dt'\right), \quad (16)$$

$$\beta = \sigma_{cb} = \frac{1}{4} \left[1 - \cos\left(2\sqrt{2} \int_{-\infty}^t \Omega(t') dt'\right) \right]. \quad (17)$$

It follows from Eq. (17) that maximal coherence $\sigma_{cb} = 0.5$ will be excited by a pair of pulses with area $S = 2\sqrt{2} \int_{-\infty}^{\infty} \Omega(t) dt = \pi$ each. Taking pulses of a Gaussian shape $\Omega = \Omega_0 \exp(-t^2/2\tau^2)$ with the area of the pulse $S = 4\sqrt{\pi}\Omega_0\tau$, we will have the maximal coherence excited when $\Omega_0\tau = \sqrt{\pi}/4 \approx 0.443$. The excited coherence will give rise to the polarization which will radiate out a coherent THz pulse. It is worth noting that this mechanism is similar to free-induction decay (FID) [29] in photon echo: excitation of a maximal coherence in a two-level system by a $\pi/2$ pulse, followed by emission of a coherent pulse. The difference is that typically in solids the FID decay is governed by the dephasing due to inhomogeneous broadening of the transition leading to decay of the corresponding coherence during the time $\sim W_{\text{inh}}^{-1}$. In the

case of ruby the THz transition is homogeneously broadened even at liquid helium temperature, so the decay of the THz coherence is determined by the homogeneous width of the corresponding transition.

For two long pulses, which can be considered as CW (in the sense that optical and THz coherences approach the steady-state), with approximately equal Rabi frequencies $\Omega_1 \approx \Omega_2$, resonant with the corresponding optical transitions, we get the THz coherence

$$\sigma_{cb} = \frac{2\Omega_2\Omega_1^* \exp\left(-\frac{6|\Omega_1|^2 t}{\gamma + (|\Omega_1|^2 + |\Omega_2|^2)/\gamma_{cb}}\right)}{\gamma_{cb}[\gamma + (|\Omega_1|^2 + |\Omega_2|^2)/\gamma_{cb}]}, \quad (18)$$

where $\gamma_{ba} = \gamma_{ca} = \gamma$ and γ_{cb} are the optical and THz coherence decay rates, respectively. In this case the maximal THz coherence $|\sigma_{cb}| = 1$ will be excited provided that $(|\Omega_1|^2 + |\Omega_2|^2) \gg \gamma\gamma_{cb}$, which is a usual steady-state EIT threshold condition.

Let us now estimate the peak intensity and energy of the optical pulses necessary to excite required coherence. The peak intensity of the pulse is expressed in terms of the peak Rabi frequency as

$$I_{\text{peak}} = \frac{2\pi\hbar c\Omega_0^2}{\gamma n\lambda\sigma_{\text{abs}}}, \quad (19)$$

where γ is the width of an optical transition, n is the refractive index at the optical wavelength, λ is the optical wavelength, and σ_{abs} is the corresponding absorption cross section. The energy of a single pulse can be calculated as

$$E_{\text{opt}} \approx \frac{2\pi\sqrt{\pi}\hbar c A_{\text{opt}} \Omega_0^2 \tau}{\gamma n\lambda\sigma_{\text{abs}}}, \quad (20)$$

where A_{opt} is the laser beam cross section.

III. PROPAGATION: PHASE-MATCHING GEOMETRY FOR FIELDS

A complete self-consistent calculation also includes field propagation equations

$$\frac{\partial \Omega_\alpha}{\partial z} + \frac{n_\alpha}{c} \frac{\partial \Omega_\alpha}{\partial t} = -\kappa_\alpha \Omega_\alpha + i\eta_\alpha \rho_\alpha, \quad (21)$$

where index $\alpha = 1, 2, 3$ indicates all fields and corresponding polarizations, $\eta_\alpha = 2\pi\omega_\alpha N \mu_\alpha^2 / n_\alpha c \hbar$ is the corresponding coupling constant, ω_α are the frequencies of the optical and THz fields, N is the density of the medium, c is the speed of light in vacuum, n_α is the corresponding refractive index, and κ_α are losses for the field during propagation in the crystal due to scattering, diffraction, or nonresonant absorption. For optical fields these losses are usually small, but for the THz field in free space the diffraction losses given by $\kappa_3 = \lambda_3 / D^2$ should be taken into account. To avoid diffraction losses the crystal can be placed in a waveguide for THz radiation, then the distribution of the field mode should be taken into account.

Propagation effects are important for nonlinear interactions such as wave mixing. Let us consider two regimes:

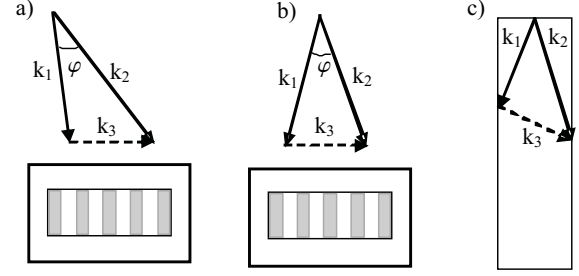


FIG. 3. (Color online) (a) CW fields 1 and 2 induce coherence between levels b and c in ruby, (b) For short pulses $k_1 = k_2$, (c) A three mode ruby laser that generates optical radiation at R_1 and R_2 lines and THz radiation simultaneously with the ruby crystal serving as a THz waveguide.

CW, when the spectral widths of pulses is smaller than the splitting between the levels of the THz transition, and the pulsed one, when the spectral width of pulses exceeds the splitting between the levels.

In the CW regime the field Ω_3 at the output of the crystal is given by (assuming that the THz pulse propagates in z direction)

$$\begin{aligned} \Omega_3 &= ie^{-\kappa_3 L} \int_0^L \eta \sigma_{cb} e^{(i\delta k + \kappa_3)z} dz = i\eta_3 \sigma_{cb} \frac{e^{i\delta k L} - e^{-\kappa_3 L}}{i\delta k + \kappa_3} \\ &= i\eta_3 \sigma_{cb} L e^{i\delta k L/2} \frac{\sin(\delta k L/2)}{(\delta k L/2)}, \end{aligned} \quad (22)$$

if losses are neglected. Here L is the length of the crystal, and the prefactor describes phase matching ($\delta k = k_{2z} - k_{1z} - k_3$). The direction of THz propagation is given by the phase-matching condition (see Fig. 3)

$$\vec{k}_2 - \vec{k}_1 = \vec{k}_3. \quad (23)$$

To satisfy the phase-matching condition $\delta k = 0$ for the THz pulse to propagate in z direction (along the crystal) the angle between the optical fields has to be adjusted according to the equation

$$k_1^2 + k_2^2 - 2k_1 k_2 \cos \phi = k_3^2, \quad \cos \phi = \frac{k_1^2 + k_2^2 - k_3^2}{2k_1 k_2}. \quad (24)$$

Rewriting a condition for optical and THz frequencies $\omega_2 - \omega_1 = \omega_3$ in the form of $k_3 = (k_2 - k_1)n_3/n_1$, we obtain

$$\phi = \sqrt{\frac{n_3^2 - n_1^2}{n_1^2}} \frac{\lambda_1}{\lambda_3}, \quad (25)$$

where $\lambda_{1(3)}$ is the wavelength of the optical (THz) field. For the case of ruby the refractive index for THz radiation is twice larger than the one for optics, $n_3 \approx 2n_{1,2}$ [25], then the angle between directions of propagation for optical fields $\phi = 3 \times 10^{-3}$. The angle between the $k_{1(2)}$ vectors and the THz field propagation direction is $\pi/3$ in this case. This provides an interesting opportunity to design a dual-wavelength ruby laser working simultaneously at R_1 and R_2 lines that can also generate THz radiation, as is shown in Fig. 3(c). The crystal will simultaneously serve as a THz waveguide in this case.

Now we turn to a short pulse excitation regime. For many femtosecond laser experimental setups it would be an interesting extension to include an option of THz generation. The phase matching in this case can be obtained by excitation of THz coherence with two optical beams with the same frequencies but different directions of propagation. It is instructive to show how it works in this case. Let us consider the problem in the simplest case of lowest order of perturbation in coherent pumping fields. The density matrix equations look as

$$\sigma_{ab}^* = -i\Omega_1 e^{-ik_x x + ik_z z} - i\Omega_2 e^{-ik_x x - ik_z z}, \quad (26)$$

$$\sigma_{ca}^* = i\Omega_1 e^{ik_x x - ik_z z} + i\Omega_2 e^{ik_x x + ik_z z}, \quad (27)$$

$$\begin{aligned} \sigma_{cb}^* = & i\sigma_{ab}[\Omega_1(t)e^{ik_x x - ik_z z} + \Omega_2(t)e^{ik_x x + ik_z z}] \\ & - i\sigma_{ca}[\Omega_1(t)e^{-ik_x x + ik_z z} + \Omega_2(t)e^{-ik_x x - ik_z z}]. \end{aligned} \quad (28)$$

A solution of this set of equations is given by

$$\begin{aligned} \sigma_{cb} = & 2 \int_{-\infty}^t dt' \int_{-\infty}^{t'} dt'' [\Omega_1(t')\Omega_1(t'') + \Omega_2(t')\Omega_2(t'') \\ & + \Omega_1(t')\Omega_2(t'')\cos 2k_z z + \Omega_1(t'')\Omega_2(t')\cos 2k_z z]. \end{aligned} \quad (29)$$

One can see that the phase-matching between the optical fields and the THz field is achieved by appropriate tilting of the optical beams at the angle $\phi \approx 2k_z/k_x = k_3/k_1 = \lambda_1 n_3/\lambda_3 n_1$; in particular, for ruby $\phi \approx 10^{-3}$.

IV. ESTIMATION OF ENERGY OF GENERATED THZ FIELD

First we analyze the optimal conditions at which the maximal THz coherence can be induced in ruby by the optical fields at both room and liquid helium temperatures. For room temperature ruby $\gamma = \gamma_{cb} = 5.5 \text{ cm}^{-1}$ [30], $n = 1.76$, $\lambda = 694.3 \text{ nm}$, and $\sigma_{\text{abs}} = 4 \times 10^{-20} \text{ cm}^2$ [22]. In the case of ultrashort driving pulses (100 fs–1 ps) the shortest THz pulse that can be generated in this system has a duration $\sim \gamma_{cb}^{-1} \sim 1 \text{ ps}$. With the optical pulses of the same duration $\tau = 1 \text{ ps}$ the Rabi frequency $\Omega_0 = 4.43 \times 10^{11} \text{ s}^{-1}$ is required to produce the maximal coherence, corresponding to $I_{\text{peak}} \sim 10^{12} \text{ W/cm}^2$, which is still below a damage threshold of ruby for such duration of the pulses [31], but we make a conservative estimate for lower intensities $I_{\text{peak}} \sim 100 \text{ GW/cm}^2$, certainly below the threshold, corresponding to the peak Rabi frequency $\Omega_0 = 2 \times 10^{11} \text{ s}^{-1}$. For long driving pulses (10 ps–1 ns) to excite the maximal coherence $|\sigma_{cb}| = 1$ would require $\Omega_{1,2}^2 \gg \gamma\gamma_{cb}$ resulting in the Rabi frequency $\Omega_{1,2} \sim 10^{12} \text{ s}^{-1}$, corresponding to intensities exceeding the ruby damage threshold for pulses of such duration. For long pulses (1–10 ns) the damage threshold intensity is in the range $I_{\text{peak}} \sim 20\text{--}30 \text{ GW/cm}^2$ [32], which corresponds to the Rabi frequency $\Omega_{1,2} \sim 10^{11} \text{ s}^{-1}$. This value is used in the estimates below.

At low temperatures (1.8–4.2 K) the THz coherence lifetime is significantly larger, $\gamma_{cb}^{-1} \sim 500 \text{ ps}$ [33], which means

that with ultrashort pumping pulses (in this case of 10 ps–1 ns duration), the maximal coherence will be excited with only $\Omega_0 \sim 10^{10} \text{ s}^{-1}$, requiring $I_{\text{peak}} \sim 100 \text{ MW/cm}^2$ pulse intensity. For long pulses (1–10 ns) the maximal coherence will be excited when $\Omega_{1,2}^2 \sim \gamma\gamma_{cb}$, and since at low temperatures $\gamma \sim 0.05 \text{ cm}^{-1}$ [34], it results in $\Omega_{1,2} \sim 5 \times 10^9 \text{ s}^{-1}$, requiring $I_{\text{peak}} \sim 30 \text{ MW/cm}^2$.

The next question is the energy of the generated THz pulse, which can be estimated from the propagation equation

$$\frac{\partial \Omega_3}{\partial z} + \frac{n_3}{c} \frac{\partial \Omega_3}{\partial t} = \frac{2\pi\omega_3 i N \mu_{cb}^2}{n_3 c \hbar} \sigma_{cb} - \kappa \Omega_3, \quad (30)$$

where N is the density of Cr^{3+} ions, $\hbar\omega_3 = 29 \text{ cm}^{-1}$ (0.87 THz), the dipole moment of the far-infrared transition can be calculated using measured experimentally low-temperature (LT) parameters $\mu_{cb}^2 = \gamma_{cb}^{\text{LT}} c \hbar n_3 \sigma_{\text{abs,THz}}^{\text{LT}} / 2\pi\omega_3$, and κ is the nonresonant absorption coefficient of the sapphire host at the THz wavelength.

Assuming that the crystal sample is side pumped homogeneously, so that the THz coherence σ_{cb} does not depend on the propagation coordinate z , and phase-matching conditions are satisfied we arrive at the equation

$$\frac{\partial \Omega_3}{\partial z} + \frac{n_3}{c} \frac{\partial \Omega_3}{\partial t} = i\eta \sigma_{cb}(t) - \kappa \Omega_3, \quad (31)$$

where $\eta = N \gamma_{cb}^{\text{LT}} \sigma_{\text{abs,THz}}^{\text{LT}}$, so that at the end of the crystal the Rabi-frequency of the THz pulse is

$$\Omega_3(t, L) = i\eta \int_{z_0}^L \sigma_{cb} \left(t - \frac{z-z'}{c} n_3 \right) e^{-\kappa(z-z')} dz', \quad (32)$$

where $z_0 = \max(0, L - tc/n_3)$. For the ultrashort pumping pulses we can model $\sigma_{cb}(t) = \sigma_{cb}^{\text{max}} \exp(-\gamma_{cb} t)$ at $t > 0$ and $\sigma_{cb} = 0$ at $t < 0$ for an estimate. Equation (32) gives

$$\Omega_3 = i\eta \sigma_{cb}^{\text{max}} \frac{e^{-\gamma_{cb} t}}{\gamma_{cb} n_3 / c - \kappa} (e^{(\gamma_{cb} n_3 / c - \kappa) t / n_3} - 1) \quad (33)$$

for $t < Ln_3/c$ and

$$\Omega_3 = i\eta \sigma_{cb}^{\text{max}} \frac{e^{-\gamma_{cb} t}}{\gamma_{cb} n_3 / c - \kappa} (e^{(\gamma_{cb} n_3 / c - \kappa) L} - 1) \quad (34)$$

for $t > Ln_3/c$.

Equations (33) and (34) then allow one to calculate the energy of the THz pulse

$$\begin{aligned} E_{\text{THz}} = & \frac{\hbar\omega_3 A}{\gamma_{cb}^{\text{LT}} n_3 \sigma_{\text{abs,THz}}^{\text{LT}}} \int_0^\infty |\Omega_3|^2 dt \\ = & \frac{\hbar\omega_3 A n^2 \gamma_{cb}^{\text{LT}} \sigma_{\text{abs,THz}}^{\text{LT}}}{n_3} (\sigma_{cb}^{\text{max}})^2 \left(\frac{1}{2\kappa\gamma_{cb}(\kappa + \gamma_{cb} n_3 / c)} \right. \\ & \left. - \frac{e^{-2\kappa L}}{2\kappa\gamma_{cb}(\gamma_{cb} n_3 / c - \kappa)} + \frac{e^{-(\kappa + \gamma_{cb} n_3 / c)L}}{\gamma_{cb}[(\gamma_{cb} n_3 / c)^2 - \kappa^2]} \right), \end{aligned} \quad (35)$$

where A is the crystal cross section along THz pulse propagation direction. For two pulses of 1 ps duration with $I_{\text{peak}} \sim 100 \text{ GW/cm}^2$ the maximal induced coherence is σ_{cb}^{max}

≈ 0.21 . Taking $N=1.6 \times 10^{19} \text{ cm}^{-3}$ for 0.05% doped ruby, and known from low-temperature measurements $\gamma_{cb}^{\text{LT}}=2 \times 10^9 \text{ s}^{-1}$, $\sigma_{\text{abs,THz}}^{\text{LT}}=3 \times 10^{-19} \text{ cm}^2$ [33], and room temperature parameters $\gamma_{cb}=10^{12} \text{ s}^{-1}$ and $\kappa=0.4-0.5 \text{ cm}^{-1}$ [25], $n_3=3.5$ [25], and considering the crystal of $1 \text{ cm} \times 1 \text{ cm} \times 0.1 \text{ cm}$ size with the $A=1 \text{ cm} \times 0.1 \text{ cm}$ THz emitting cross section and $L=1 \text{ cm}$ length, we arrive at $E_{\text{THz}} \approx 630 \text{ pJ}$. The energy can be higher for higher optical peak intensities, approaching several nJ for $I_{\text{peak}} \sim 10^{12} \text{ W/cm}^2$. For low temperatures (1.8–4.2 K) the parameters are: $\gamma_{cb}=2 \times 10^9 \text{ s}^{-1}$, $\sigma_{\text{abs,THz}}=3 \times 10^{-19} \text{ cm}^2$, $\kappa=0.01 \text{ cm}^{-1}$ [25], and the maximal coherence $\sigma_{cb}=0.5$ can be easily excited. Due to stronger absorption at low temperatures ($\sigma_{\text{abs}} \sim 10^{-18} \text{ cm}^2$ [22]), half of the optical intensity will be absorbed at $\approx 0.5 \text{ mm}$ for 0.05% Cr^{3+} density, therefore, for this estimate we take a crystal with dimensions $1 \text{ cm} \times 0.1 \text{ cm} \times 0.05 \text{ cm}$ size with the THz emitting cross section $A=0.1 \text{ cm} \times 0.05 \text{ cm}$ and $L=1 \text{ cm}$ length which results in $E_{\text{THz}} \sim 7.5 \text{ }\mu\text{J}$.

Let us also make an estimate for fs pulse duration. Since powerful fs Ti:sapphire lasers are readily available in many laboratories nowadays this is of interest. In this case the coherence can be excited by just one pulse of 100 fs duration, since its spectral width is larger than the THz transition splitting. Although, to satisfy phase-matching conditions, it is necessary to split it in two beams hitting the crystal at slightly different angles. Keeping the same peak intensity $I_{\text{peak}} \approx 100 \text{ GW/cm}^2$ we obtain a smaller pulse area $S=0.14$, giving the coherence $\sigma_{cb}^{\text{max}} \sim 2.5 \times 10^{-3}$ and resulting in THz pulse energy of $\approx 100 \text{ fJ}$ at room temperature.

For the CW pumping case we have, in analogy with the short pulse pumping

$$E_{\text{THz}} = \frac{\hbar \omega_3 A N^2 \gamma_{cb}^{\text{LT}} \sigma_{\text{abs,THz}}^{\text{LT}} (\sigma_{cb}^{\text{max}})^2 \left(\frac{1}{2\kappa G(\kappa + Gn_3/c)} - \frac{e^{-2\kappa L}}{2\kappa G(Gn_3/c - \kappa)} + \frac{e^{-(\kappa + Gn_3/c)L}}{G[(Gn_3/c)^2 - \kappa^2]} \right)}{n_3} \quad (36)$$

where from Eq. (18) $\sigma_{cb}^{\text{max}}=2\Omega_2^* \Omega_1 / (\gamma\gamma_{cb} + |\Omega_1|^2 + |\Omega_2|^2)$ and $G=6|\Omega_1|^2 / [\gamma + (|\Omega_1|^2 + |\Omega_2|^2) / \gamma_{cb}]$. In the limit $\Omega_{1,2}^2 \gg \gamma\gamma_{cb}$ the maximal coherence is excited $\sigma_{cb}=1$, which would require, though, experimentally unfeasible Rabi frequency $\Omega_{1,2} \sim 10^{12} \text{ s}^{-1}$ at room temperature, resulting in $I_{\text{peak}} \sim 10^{12} \text{ W/cm}^2$. For such long pulses (10 ps–1 ns) the damage threshold intensity for ruby is $I^{\text{peak}} \sim 20-30 \text{ GW/cm}^2$, which corresponds to the Rabi frequency $\Omega_{1,2} \sim 10^{11} \text{ s}^{-1}$. For this Rabi frequency and room temperature decay rates $\gamma \approx \gamma_{cb}=10^{12} \text{ s}^{-1}$, the ratio $\Omega_{1,2}^2 / \gamma\gamma_{cb} \sim 10^{-2}$ and the resulting THz coherence $|\sigma_{cb}| \sim 10^{-2}$ for a 10 ps pulse. The THz pulse energy will be $E_{\text{THz}} \sim 300 \text{ pJ}$. At low temperatures the maximal coherence $\sigma_{cb}=1$ can be excited by long pulses (1–10 ns), which would give energy of a THz pulse $E_{\text{THz}} \sim 8 \text{ }\mu\text{J}$.

Finally we estimate the total energy of optical pulses using Eq. (20) and overall conversion efficiency to THz radiation. For room temperature 1 ps pulses pumping the side of the crystal with $A_{\text{opt}}=1 \text{ cm} \times 0.1 \text{ cm}$ size, the energy in one pulse according to Eq. (20) is $E_{\text{opt}} \approx 27 \text{ mJ}$, for two pulses, 54 mJ, respectively. We have to take into account that only

TABLE I. Estimates of the THz pulse energy, peak THz field amplitude, required optical pulse parameters and THz radiation generation efficiency in ruby at room temperature

Ultrashort 100 fs	pulses (100 fs–1 ps) 1 ps	long pulses (10 p–100 ps) 10 ps
$\sigma_{cb} \sim 2.5 \cdot 10^{-3}$	$\sigma_{cb}=0.21$	$\sigma_{cb} \sim 10^{-2}$
$E_{\text{THz}} \sim 100 \text{ fJ}$	$E_{\text{THz}} \sim 630 \text{ pJ}$	$E_{\text{THz}} \sim 300 \text{ pJ}$
$\mathcal{E}_{\text{THz}} \sim 300 \text{ V/cm}$	$\mathcal{E}_{\text{THz}} \sim 23 \text{ kV/cm}$	$\mathcal{E}_{\text{THz}} \sim 5 \text{ kV/cm}$
$\Omega_0=2 \times 10^{11} \text{ s}^{-1}$	$\Omega_0=2 \times 10^{11} \text{ s}^{-1}$	$\Omega_0 \sim 10^{11} \text{ s}^{-1}$
$I_{\text{peak}}=100 \text{ GW/cm}^2$	$I_{\text{peak}}=100 \text{ GW/cm}^2$	$I_{\text{peak}}=20-30 \text{ GW/cm}^2$
$E_{\text{opt}}=110 \text{ mJ}$	$E_{\text{opt}}=11 \text{ mJ}$	$E_{\text{opt}} \sim 300 \text{ mJ}$
$^a \eta \sim 6 \times 10^{-9}$	$\eta \sim 10^{-11}$	$\eta \sim 10^{-8}$

^aEfficiency is estimates as a ratio of the THz pulse energy to the total energy of optical pulses absorbed in the crystal $\eta = E_{\text{THz}}/2E_{\text{opt}}$. The ultimate efficiency of the method is given by the ratio of the THz radiation frequency to the frequency of the optical transition $29 \text{ cm}^{-1}/14420 \text{ cm}^{-1}=2 \times 10^{-3}$.

$[1 - \exp(-\sigma_{\text{abs}} N L_{\text{opt}})]$ of the incident energy is absorbed, where L_{opt} is the size of the crystal along which the optical pulses propagate. For room temperature $\sigma_{\text{abs}}=4 \times 10^{-20} \text{ cm}^2$, $N=1.6 \times 10^{19} \text{ cm}^{-3}$, and $L_{\text{opt}}=1 \text{ cm}$, the absorbed fraction is 0.47, so about twice the energy calculated above is required, resulting in $\sim 110 \text{ mJ}$ total energy. For a pair of 100 fs pulses the same reasoning leads to the total energy of $\sim 11 \text{ mJ}$ [2.7 mJ in one pulse from Eq. (20)]. For long pulses the total required energy is 300 mJ.

The expected values of the energy of THz pulses, the peak amplitude of the THz field if focused to a spot of $300 \text{ }\mu\text{m}$ size, required pumping radiation energy and duration and efficiency of optical to THz energy conversion for room temperature ruby are summarized in Table I.

At low temperatures as was already discussed above 55% of optical intensity is absorbed at $L_{\text{opt}}=0.05 \text{ cm}$. Taking $A_{\text{opt}}=1 \text{ cm} \times 0.1 \text{ cm}$ we obtain from Eq. (20) for short pulses $E_{\text{opt}} \approx 13.5 \text{ mJ}$ in one pulse, giving total required energy of 54 mJ. For long pulses the estimate gives $E_{\text{opt}}=67.5 \text{ mJ}$ in one pulse and 270 mJ total energy for long pulses. The parameters of THz pulses: energy, peak amplitude if focused to a spot of $300 \text{ }\mu\text{m}$ size, and required optical pulses energy and duration at low temperatures are summarized in Table II.

V. DISCUSSION

A. Application to other solid materials

It is important to note that the proposed technique can be applied to other solid materials with suitable transitions in the THz range. Similar schemes can be found in other ions as well, since for a typical rare-earth or transition metal ion the level structure is complex, having many crystal field and spin-orbit split components, separated by tens to hundreds of wave numbers. For example, this method is readily applicable to $\text{Cr}^{3+}:\text{BeAl}_2\text{O}_4$ (alexandrite), having R line splittings of 41 cm^{-1} (1.23 THz) in a noninversion Cr^{3+} site [35], and R line absorption-emission cross sections ten times larger

TABLE II. Estimates of the THz pulse energy, peak THz field amplitude, required optical pulse parameters and efficiency of THz radiation generation in ruby at low temperatures

Ultrashort pulses (10 ps–1 ns)	long pulses (1 s–10 ns)
$\sigma_{cb}=0.5$	$\sigma_{cb}=1$
$E_{\text{THz}}\sim 7.5 \mu\text{J}$	$E_{\text{THz}}\sim 8 \mu\text{J}$
$\mathcal{E}_{\text{THz}}\sim 230 \text{ kV/cm}$	$\mathcal{E}_{\text{THz}}\sim 170 \text{ kV/cm}$
$\Omega_0=10^{10} \text{ s}^{-1}$	$\Omega_0\sim 5\times 10^9 \text{ s}^{-1}$
$I_{\text{peak}}=100 \text{ MW/cm}^2$	$I_{\text{peak}}=30 \text{ MW/cm}^2$
$E_{\text{opt}}=54 \text{ mJ}$	$E_{\text{opt}}\sim 270 \text{ mJ}$
$\eta\sim 10^{-4}$	$\eta\sim 3\times 10^{-5}$

than ruby ($3\times 10^{-19} \text{ cm}^2$ at room temperature). It allows one to decrease peak optical intensities to induce maximal THz coherence and results in higher conversion efficiency.

The technique can also be applied to rare-earth ion doped materials, for example, Pr^{3+} doped hosts, such as LaF_3 [36], Y_2SiO_5 [37], CaF_2 [38] with the ground and excited state Stark splittings being in a broad range 17–100 cm^{-1} and higher, the same splittings are found in Nd^{3+} doped crystals, such as YAG [39] and YVO_4 [40], and a number of others, for example Tm:YAG [41] and Er:YAG [42] and Er:YLiF₄ [43].

Also it is important to note that the technique can be applied to gases as well, but the coupling to THz radiation in this case occurs by a magnetic-dipole moment (macroscopic polarization due to an electric-dipole moment is zero because of symmetry reasons). Typically the magnetic dipole moment is smaller than the electric dipole one, so efficiency is smaller, but for higher densities and pressures this approach can still produce THz radiation. The dipole moments for optical transitions can be stronger than for ruby, so the coherence can be larger. This possibility is an extension of the method proposed in Refs. [5,6], although its analysis is beyond of the scope of the present paper.

The next important remark is related to the case when the THz transition of interest belongs to the ground state. Then there are a lot of new opportunities to use more sophisticated methods of coherence preparation. In particular, the method of pulsed coherence production via stimulated Raman adiabatic passage (STIRAP) [44] can be used to control the duration of the THz pulse similarly to [6]. Generally, all methods for coherence preparation via femtosecond pulse shaping developed to improve the sensitivity of coherent Raman scattering [16], in particular, frequency chirping [16] and fractional STIRAP [15], matched pulses [45], etc., can be applied.

B. Comparison with current methods of short THz pulse generation

It is interesting to compare the method of THz generation proposed in recent works [5,6] and in this paper with currently available ones. There are a variety of methods already considered successful for generation of short THz pulses, so

it is worth to compare the above estimates with the currently achieved parameters.

At the moment the most impressive results in generation of short THz pulses were achieved using electron beam based sources, free-electron lasers (FEL) [46,47] and synchrotrons [48,49]. For FELs, typically THz pulses of about 1 ps duration with 1–40 ns distance between micropulses are generated, grouped into a few- μs trains. Energies of the micropulses are about 1–50 mJ (the parameters of FELBE laser, Rossendorf, Germany). Recently, substantially higher powers of coherent broadband THz pulses, produced by synchrotron emission, were obtained from the electron beamline [48,49]. Hundreds of fs-short half-cycle THz pulses were generated with energies up to 100 μJ .

THz pulses with ns durations were achieved in THz semiconductor lasers (quantum cascade lasers and p -Ge and n -Si lasers [50–54]), limited by the need of cryogenic cooling and in the case of p -Ge lasers by high electric and magnetic fields required for laser operation. In p -Ge lasers [51–53] 20 ps pulse durations were obtained in a mode-locked regime with peak power up to several Watts in a few- μs train of pulses.

The obvious advantages of the optical crystal based THz emitters discussed in this work over FEL and synchrotron sources are compactness (typical optical solid-state materials are significantly smaller), cost, and ease of handling. Compared to THz QC lasers the crystals are much easier to grow and handle, they also can provide better coupling between the THz mode and the generating material due to a larger size of crystals.

Other methods of short THz pulse generation are based on interaction of different materials with ultrashort laser pulses. The most popular ones, giving subpicosecond THz pulses, are the photocurrent method using the Auston-switch technique [55] and the optical rectification technique [56]. Since the proposed crystal-based THz sources are closer in their characteristics to these methods, we will make a more detailed comparison. Recently THz sources based on amplifier-laser systems such as Ti:sapphire, utilizing different methods of THz radiation generation such as optical rectification in nonlinear crystals and laser-produced plasma and photocurrent THz generation in semiconductor antennas, became popular. The transition metal and rare-earth ion doped crystals proposed in this work as THz emitters are suitable for amplifier-laser-based THz systems working in a single-shot regime [57], since the typically long (hundreds μs –ms) population decay time of excited states of these ions limits the repetition rate. Crystals are also better in terms of saturation, able to withstand high laser pulse fluence and thus very compatible with low-repetition rate table-top laser systems producing pulses with energies in the 10–100 mJ range with ~ 10 Hz repetition rates. Figure 4 compares the predicted in Ref. [57] performance of different amplifier-laser-based THz sources and ruby at room temperature, at optical pulses energy of ~ 10 mJ. It shows that ruby is expected to perform as good as the biased GaAs antenna with 1 kV/cm dc bias field and the plasma THz source with an external bias field, slightly yielding them in conversion efficiency.

Figure 5 compares the predicted in Ref. [57] performance of different amplifier-laser-based THz sources at room tem-

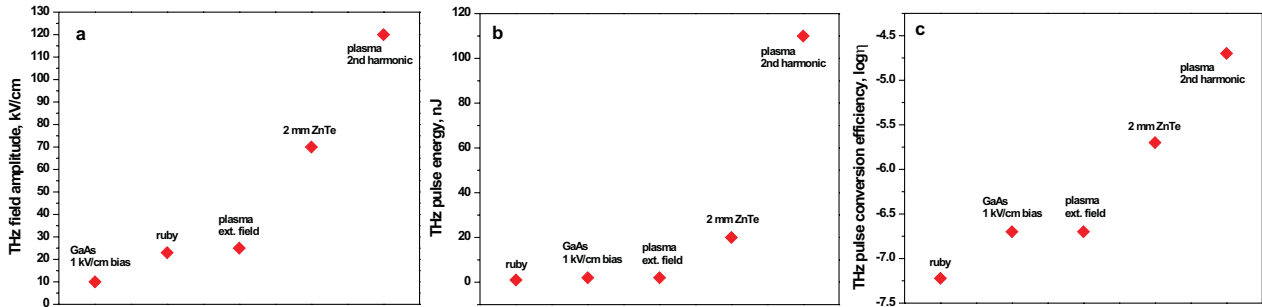


FIG. 4. (Color online) Predicted in Ref. [57] performance of several amplifier-laser-based THz sources and ruby at room temperature with optical pulses energy ~ 10 mJ: (a) peak THz field amplitude, (b) THz pulse energy, (c) conversion efficiency.

perature and ruby at liquid helium one, at optical pulses energy of ~ 100 mJ. The ruby source at liquid helium temperature can compete with the plasma source utilizing the fundamental and second harmonic optical fields in terms of THz pulse energy and conversion efficiency, and yields it in peak THz field amplitude.

C. Advantages of the technique

New methods of THz generation proposed in Refs. [4–6] for atomic and molecular gases and in the present work for doped crystals potentially have very high efficiency, they offer the possibility of THz pulses with controlled durations including femtosecond region and the possibility of generation of pulses with high energy, already comparable with synchrotron or free-electron laser based THz sources. Implementation of the method, therefore, will open exciting opportunities in many fields of THz applications such as the time-resolved THz spectroscopy. Using intense short pulses of THz radiation generated by the proposed method will significantly increase the performance of spectroscopic measurements, allowing maximal (among currently existing methods) temporal resolution. Extremely high efficiency of the proposed technique opens a way for orders of magnitude increase in sensitivity of the spectroscopic methods, THz tomography, nondestructive quality control, medical diagnostics, and biomaterial characterization.

Another advantage of the proposed scheme is a better control over the phase of the generated THz radiation, resulting in lower (pulse duration \times bandwidth) product compared to the noncoherent techniques. Resulting THz pulses have narrower bandwidth, thus offering an opportunity of better resolution measurements. Coherence of the generated THz pulses combined with their high energy opens the way to various nonlinear phenomena in the THz range, as well as to coherent phenomena similar to the ones observed with lasers in the visible range, such as Rabi oscillations, coherent transients, etc. The proposed methods have, therefore, high potential for investigation of nonlinear effects in chemical and biological objects, in medical applications, which is a substantial, practically unexplored field of research.

VI. CONCLUSION

In the present work we proposed a technique for the generation of short intense THz pulses in coherently driven doped optical crystals. The method is based on excitation of maximal THz coherence by a pair of resonant optical pulses, resulting in polarization buildup in the medium, which will radiate a THz pulse. As an example, a well-known laser

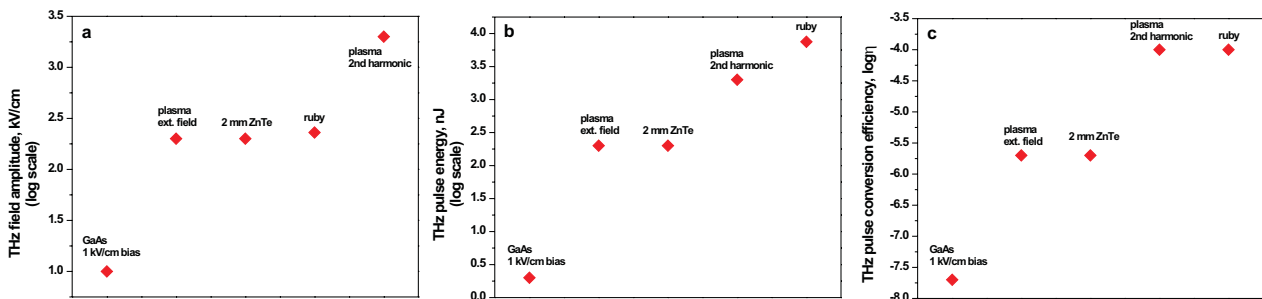


FIG. 5. (Color online) Predicted in Ref. [57] performance of several amplifier-laser-based THz sources at room temperature and ruby at liquid helium one with optical pulses energy ~ 100 mJ: (a) peak THz field amplitude, (b) THz pulse energy, (c) conversion efficiency.

material $\text{Cr}^{3+}:\text{Al}_2\text{O}_3$ (ruby) is considered and numerical estimates of expected THz and required optical field parameters are given. A number of other doped crystals, having transitions in the THz range, are suggested. Comparison is made with the existing methods of short THz pulses generation.

In summary, the optical crystal based THz sources proposed in this work can potentially produce short high energy (hundreds pJ–tens μJ) THz pulses with durations ranging from 1 ps up to several ns. The generated THz radiation will be coherent, thus offering the possibility of coherent interaction between the THz pulses and probed media. This allows

one to study various types of nonlinear phenomena. Obvious advantages of crystals are their compact size, ease of growth and handling, robustness, and low cost.

ACKNOWLEDGMENTS

We gratefully acknowledge the support from the Air Force Office of Scientific Research, the National Science Foundation, the Defense Advanced Research Projects, the Office of Naval Research under Grant No. N00014-03-1-0385, and the Robert A. Welch Foundation (Grant No. A1261).

-
- [1] *Terahertz Optoelectronics*, edited by K. Sakai (Springer, Berlin, 2005); B. Ferguson, and X.-C. Zhang, *Nat. Mater.* **1**, 26 (2002).
- [2] *Sensing with Terahertz Radiation*, edited by D. Mittleman (Springer, New York, 2003).
- [3] N. G. Kalugin, in *Handbook of Semiconductor Nanostructures and Nanodevices*, edited by A. A. Balandin and K. L. Wang (American Scientific Publishers, Los Angeles, 2005).
- [4] A. S. Zibrov, M. D. Lukin, L. Hollberg, and M. O. Scully, *Phys. Rev. A* **65**, 051801(R) (2002).
- [5] N. G. Kalugin, Y. Rostovtsev, M. O. Scully, *Proc. SPIE* **6120**, 612002 (2006); N. G. Kalugin, Y. Rostovtsev, and M. O. Scully, *quant-physics/0602142*.
- [6] N. G. Kalugin and Y. Rostovtsev, *Opt. Lett.* **31**, 969 (2006).
- [7] O. Kocharovskaya and Ya. I. Khanin, *Pis'ma Zh. Eksp. Teor. Fiz.* **48**, 581 (1988) [*Sov. Phys. JETP* **48**, 630 (1988)]; S. E. Harris, *Phys. Rev. Lett.* **62**, 1033 (1989); M. O. Scully, S. Y. Zhu, and A. Gavrielides, *ibid.* **62**, 2813 (1989).
- [8] E. Arimondo in *Progress in Optics XXXV*, edited by E. Wolf (Elsevier, Amsterdam, 1996), p. 257; S. E. Harris, *Phys. Today* **50**, 36 (1997).
- [9] A. S. Zibrov, M. D. Lukin, D. E. Nikonov, L. Hollberg, M. O. Scully, V. L. Velichansky, H. G. Robinson, *Phys. Rev. Lett.* **75**, 1499 (1995); G. G. Padmabandu, G. R. Welch, I. N. Shubin, E. S. Fry, D. E. Nikonov, M. D. Lukin, and M. O. Scully, *ibid.* **76**, 2053 (1996).
- [10] G. Alzetta, A. Gozzini, L. Moi, and G. Orriols, *Nuovo Cimento Soc. Ital. Fis., B* **36**, 5 (1976); H. R. Gray, R. M. Whitley, and C. R. Stroud, Jr., *Opt. Lett.* **3**, 218 (1978); K. J. Boller, A. Imamoglu, and S. E. Harris, *Phys. Rev. Lett.* **66**, 2593 (1991); J. E. Field, K. H. Hahn, and S. E. Harris, *ibid.* **67**, 3062 (1991).
- [11] S. E. Harris and M. Jain, *Opt. Lett.* **22**, 636 (1997).
- [12] R. W. Boyd and M. O. Scully, *Appl. Phys. Lett.* **77**, 3559 (2000).
- [13] M. Jain, H. Xia, G. Y. Yin, A. J. Merriam, and S. E. Harris, *Phys. Rev. Lett.* **77**, 4326 (1996).
- [14] O. Kocharovskaya, R. Kolesov, and Yu. Rostovtsev, *Phys. Rev. Lett.* **82**, 3593 (1999).
- [15] V. A. Sautenkov, C. Y. Ye, Y. V. Rostovtsev, G. R. Welch, and M. O. Scully, *Phys. Rev. A* **70**, 033406 (2004).
- [16] M. O. Scully, G. W. Kattawar, P. R. Lucht, T. Opatrny, H. Pilloff, A. Rebane, A. V. Sokolov, and M. S. Zubairy, *Proc. Natl. Acad. Sci. U.S.A.* **9**, 10994 (2002).
- [17] E. Kuznetsova, O. Kocharovskaya, P. Hemmer, and M. O. Scully, *Phys. Rev. A* **66**, 063802 (2002).
- [18] E. Kuznetsova, R. Kolesov, and O. Kocharovskaya, *Phys. Rev. A* **70**, 043801 (2004).
- [19] R. Kolesov, E. Kuznetsova, and O. Kocharovskaya, *Phys. Rev. A* **71**, 043815 (2005).
- [20] M. D. Frogley, J. F. Dynes, M. Beck, J. Faist, and C. C. Phillips, *Nat. Mater.* **5**, 175 (2006).
- [21] D. S. Pestov, A. A. Belyanin, V. V. Kocharovskiy, V. V. Kocharovskiy, and M. O. Scully, *J. Mod. Opt.* **51**, 2523 (2004).
- [22] D. F. Nelson and M. D. Sturge, *Physica (Amsterdam)* **137**, A1117 (1965).
- [23] H. Lengfellner and K. F. Renk, *IEEE J. Quantum Electron.* **13**, 421 (1977).
- [24] A. A. Kaplyanskii and S. A. Basun, in *Nonequilibrium Phonons in Nonmetallic Crystals*, edited by W. Eisenmenger and A. A. Kaplyanskii (North-Holland, Amsterdam, 1986), p. 373.
- [25] N. M. Lawandy, *IEEE J. Quantum Electron.* **15**, 401 (1979).
- [26] D. W. Faries, P. L. Richards, Y. R. Shen, and K. H. Yang, *Phys. Rev. A* **3**, 2148 (1971).
- [27] T. Yajima and K. Inoue, *Phys. Lett.* **26A**, 281 (1968).
- [28] M. O. Schweika-Kresimon, J. Gutschank, and D. Suter, *Phys. Rev. A* **66**, 043816 (2002).
- [29] R. G. Brewer and R. L. Shoemaker, *Phys. Rev. A* **6**, 2001 (1972).
- [30] B. Halperin, J. A. Koningstein, and D. Nicollin, *Chem. Phys. Lett.* **68**, 58 (1979).
- [31] S. A. Belozarov, G. M. Zverev, V. S. Naumov, and V. A. Pashkov, *Sov. Phys. JETP* **35**, 158 (1972).
- [32] G. M. Zverev, T. N. Mikhailova, V. A. Pashkov, and N. M. Solov'eva, *Sov. Phys. JETP* **26**, 1053 (1968).
- [33] N. Retzer, H. Lengfellner, and K. F. Renk, *Phys. Lett.* **96A**, 487 (1983).
- [34] D. E. McCumber and M. D. Sturge, *J. Appl. Phys.* **34**, 1682 (1963).
- [35] J. C. Walling, O. G. Peterson, H. P. Jenssen, R. C. Morris, and E. W. O'Dell, *IEEE J. Quantum Electron.* **16**, 1302 (1980).
- [36] R. M. Shelby, R. M. Macfarlane, and C. S. Yannoni, *Phys. Rev. B* **21**, 5004 (1980).

- [37] R. W. Equall, R. L. Cone, and R. M. Macfarlane, *Phys. Rev. B* **52**, 3963 (1995).
- [38] R. M. Macfarlane, D. P. Burum, and R. M. Shelby, *Phys. Rev. B* **29**, 2390 (1984).
- [39] G. W. Burdick, C. K. Jayasankar, F. S. Richardson, and M. F. Reid, *Phys. Rev. B* **50**, 16 309 (1994).
- [40] D. K. Sandar and R. M. Yow, *Opt. Mater.* **14**, 5 (2000).
- [41] R. M. Macfarlane, *J. Lumin.* **85**, 181 (2000).
- [42] J. B. Gruber, J. R. Quagliano, M. F. Reid, F. S. Richardson, M. E. Hills, M. D. Seltzer, S. B. Stevens, C. A. Morrison, and T. H. Allik, *Phys. Rev. B* **48**, 15561 (1993).
- [43] R. A. Macfarlane, *J. Opt. Soc. Am. B* **8**, 2009 (1991).
- [44] K. Bergmann, H. Theuer, and B. W. Shore, *Rev. Mod. Phys.* **70**, 1003 (1998).
- [45] G. Beadie, Z. E. Sariyanni, Y. V. Rostovtsev, T. Opatrny, J. Reintjes, and M. O. Scully, *Opt. Commun.* **244**, 423 (2005).
- [46] G. P. Williams, *Rep. Prog. Phys.* **69**, 301 (2006).
- [47] V. S. Cherkassky, B. A. Knyazev, V. V. Kubarev, G. N. Kulipanov, G. L. Kuryshv, A. N. Matveenkov, A. K. Petrov, V. M. Popik, M. A. Scheglov, O. A. Shevchenko, and N. A. Vinokurov, *Nucl. Instrum. Methods Phys. Res. A* **543**, 102 (2005).
- [48] G. R. Neil, G. L. Carr, J. F. Gubeli, K. Jordan, M. C. Martin, W. R. McKinney, M. Shinn, M. Tani, G. P. Williams, and X. C. Zhang, *J. Phys. Chem.* **122**, 054317 (2005).
- [49] G. L. Carr, M. C. Martin, W. R. McKinney, K. Jordan, G. R. Neil, and G. P. Williams, *J. Biol. Phys.* **29**, 319 (2003).
- [50] R. Koehler, A. Tredicucci, F. Bertram, H. E. Beere, E. H. Linfield, A. G. Davies, D. A. Ritchie, R. C. Iotti, and R. F. Rossi, *Nature (London)* **417**, 156 (2002).
- [51] A. A. Andronov, I. V. Zverev, V. A. Kozlov, Yu. N. Nozdrin, S. A. Pavlov, and V. N. Shastin, *JETP Lett.* **40**, 804 (1984); E. Gornik and A. A. Andronov, *Opt. Quantum Electron.* **23**, S111 (1991).
- [52] V. I. Gavrilenko, N. G. Kalugin, Z. E. Krasilnik, V. V. Nikonorov, A. V. Galyagin, and P. N. Tsereteli, *Semicond. Sci. Technol.* **7**, B649 (1992).
- [53] A. V. Muravjov, R. C. Stribos, C. J. Fredricksen, H. Weidner, W. Trimble, S. G. Pavlov, V. N. Shastin, and R. E. Peale, *Appl. Phys. Lett.* **73**, 3037 (1998).
- [54] S. G. Pavlov, R. K. Zhukavin, E. E. Orlova, V. N. Shastin, A. V. Kirsanov, H. W. Hubers, K. Auen, and H. Riemann, *Phys. Rev. Lett.* **84**, 5220 (2000).
- [55] X.-C. Zhang, B. B. Hu, J. T. Darrow, and D. H. Auston, *Appl. Phys. Lett.* **56**, 1011 (1990); D. H. Auston, K. P. Cheung, and P. R. Smith, *ibid.* **45**, 284 (1984).
- [56] K. H. Yang, P. L. Richards, and Y. R. Shen, *Appl. Phys. Lett.* **19**, 320 (1971); A. Rice, X. F. Ma, X.-C. Zhang, D. Bliss, J. Larkin, and M. Alexander, *ibid.* **64**, 1324 (1994).
- [57] T. Löffler, M. Krebs, M. Thomson, T. Hahn, N. Hasegawa, and H. G. Roskos, *Semicond. Sci. Technol.* **20**, S134 (2005).